

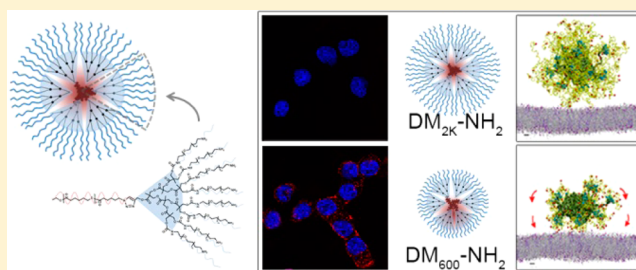
# Poly(ethylene glycol) Corona Chain Length Controls End-Group-Dependent Cell Interactions of Dendron Micelles

Hao-jui Hsu,<sup>†</sup> Soumyo Sen,<sup>§</sup> Ryan M. Pearson,<sup>†</sup> Sayam Uddin,<sup>†</sup> Petr Král,<sup>§,||</sup> and Seungpyo Hong<sup>\*,†,‡</sup>

<sup>†</sup>Departments of Biopharmaceutical Sciences, <sup>‡</sup>Bioengineering, <sup>§</sup>Chemistry, and <sup>||</sup>Physics, University of Illinois at Chicago, Chicago, Illinois 60612, United States

## Supporting Information

**ABSTRACT:** To systematically investigate the relationship among surface charge, PEG chain length, and nano–bio interactions of dendron-based micelles (DMs), a series of PEGylated DMs with various end groups ( $-\text{NH}_2$ ,  $-\text{Ac}$ , and  $-\text{COOH}$ ) and PEG chain lengths (600 and 2000 g/mol) are prepared and tested *in vitro*. The DMs with longer PEG chains ( $\text{DM}_{2\text{K}}$ ) do not interact with cells despite their positively charged surfaces. In sharp contrast, the DMs with shorter PEG chains ( $\text{DM}_{600}$ ) exhibit charge-dependent cellular interactions, as observed in both *in vitro* and molecular dynamics (MD) simulation results. Furthermore, all DMs with different charges display enhanced stability for hydrophobic dye encapsulation compared to conventional linear-block copolymer-based micelles, by allowing only a minimal leakage of the dye *in vitro*. Our results demonstrate the critical roles of the PEG chain length and polymeric architecture on the terminal charge effect and the stability of micelles, which provides an important design cue for polymeric micelles.



## INTRODUCTION

Surface immobilization of poly(ethylene glycol) (PEG), or PEGylation, is widely used to modify nanoparticles (NPs) with the goal to avoid undesired, nonspecific biological interactions. The covalent attachment of PEG to NPs results in the formation of a relatively inert hydrophilic corona that reduces uptake by the reticuloendothelial system, thereby prolonging the circulation time of NPs such as therapeutic proteins, dendrimers, liposomes, and micelles.<sup>1–3</sup> It has been reported that the length of PEG chains plays a major role in determining the cellular interaction of PEGylated NPs because it affects the particle size, PEG conformation (mushroom vs brush), and thickness and surface coverage of the PEG corona.<sup>4–6</sup> The surface charge of NPs is another important parameter that can affect cellular interactions of NPs. In general, NPs with positively charged surfaces (e.g.,  $-\text{NH}_2$  termini that are protonated under physiological pH) are known to nonspecifically interact with cells and cause toxicity via membrane destabilization, which can be typically diminished by charge neutralization or carboxylation.<sup>7–9</sup> In particular, poly-(amidoamine) (PAMAM) dendrimers have been extensively used to study charge-dependent cellular interactions because of their chemically well-defined, dendritic structure that amplifies the effect of surface groups.<sup>9–17</sup> Although the effects of PEG corona and surface charges of NPs on their cellular interactions have been widely studied independently, it has not been fully understood to date how they collectively affect the nano–bio interactions.

Our group recently synthesized amphiphilic PEGylated dendron-based copolymers (PDCs) consisting of hydrophobic

poly( $\epsilon$ -caprolactone) (PCL), polyester dendron, and multiple hydrophilic PEG chains.<sup>18</sup> When the self-assembly characteristics of PDCs were compared to those of similar linear-block copolymers (LBCs), PDCs displayed critical micelle concentrations (CMC) ( $\sim 10^{-7}$ – $10^{-8}$  M) that were up to 2 orders of magnitude lower than LBCs, indicating their enhanced thermodynamic stability.<sup>18</sup> Molecular dynamics (MD) simulations also revealed that the dendron micelles (DMs) were almost completely covered by a dense PEG layer, whereas LBC-based micelles displayed a considerable degree of PCL core exposure at their surface. This difference was attributed to the high-density PEG layers provided by the dendritic architecture of PDCs. Interestingly, unlike PAMAM dendrimers, after the termini of the PEG (2000 g/mol) chains of the PDCs were modified to primary amines, the resulting DMs ( $\text{DM}_{2\text{K}}-\text{NH}_2$ ) did not exhibit any noticeable cellular interactions or toxicity.<sup>19</sup> This charge-independent end-group effect of the  $\text{DM}_{2\text{K}}-\text{NH}_2$  was attributed to a 10-fold higher molecular-weight-to-charge-number of the PDCs than that of PAMAM dendrimers and back-folding of the terminal amines into the ethylene glycol ( $-\text{CH}_2\text{CH}_2\text{O}-$ ) backbone. These results demonstrated that the long PEG chain contributes to the sequestration of charge-dependent end-group effects of the DMs.

Our previous findings raised a vital question of whether the end-group charge effects of DMs could be tuned through

Received: June 17, 2014

Revised: September 15, 2014

Published: September 30, 2014

changing the PEG chain length. To address this question, we hypothesized that the lack of charge-dependent end-group effects of DM<sub>2K</sub>-NH<sub>2</sub> could turn to be charge-dependent by shortening the PEG chain lengths. In this study, we synthesized a series of PDCs with shorter PEG chains (600 g/mol) (PDC<sub>600</sub>) and investigated the relation between the length of PEG chains and the end-group charge effect of DMs on their cellular interactions. The DM–membrane interactions were further studied in atomistic detail using MD simulations. In addition, the effect of polymeric architecture on the encapsulation stability of the resulting micelles was investigated. By comparing DMs and LBC-based micelles (LMs) encapsulating a membrane permeable fluorescent dye, its leakage kinetics from the two types of micelles was evaluated. This study presents a systematic investigation of the effect of surface charge, PEG chain length, and polymeric architecture on the cellular interactions and stability of polymeric micelles.

## EXPERIMENTAL SECTION

**Materials.** BOC PEG amine, HCl salt (BOC-PEG<sub>600</sub>-NH<sub>2</sub>) (MW 600 g/mol), was purchased from JenKem Technology USA Inc. (Plano, TX). Rhodamine-NHS was purchased from Pierce (Rockford, IL). Regenerated cellulose dialysis membrane (3.5 kg/mol MWCO) was purchased from Spectrum Laboratories (Rancho Dominguez, CA). Generation 4 (G4) PAMAM dendrimers and all other reagents were purchased from Sigma-Aldrich Co. (St. Louis, MO) and used without further purification unless specified otherwise.

**Synthesis of End-Group-Modified PDC<sub>600</sub>.** Amine-reactive PCL<sub>3,5K</sub>-G3-PNP (4-nitrophenyl ester) was synthesized according to our published protocol<sup>18</sup> followed by PEGylation. Briefly, PCL<sub>3,5K</sub>-G3-PNP (150 mg, 0.026 mmol) was dissolved in dimethylformamide (DMF) (4 mL) for 2 h and added into NH<sub>2</sub>-PEG<sub>600</sub>-BOC (150 mg, 0.249 mmol) in DMF (3 mL) in the presence of triethylamine (TEA) (84.17 mg, 0.832 mmol). The reaction was carried out at room temperature for 24 h. The reaction mixture was then transferred to a dialysis membrane (3.5 kg/mol MWCO), dialyzed against distilled water (dH<sub>2</sub>O) for 48 h with five water changes, and lyophilized using a FREEZONE 4.5 freeze-dryer (LABCONCO Corp., Kansas City, MO) for 2 days. The resulting PCL<sub>3,5K</sub>-G3-PEG<sub>600</sub>-BOC was obtained as powder. To remove the BOC protecting groups in the product, a solution of PCL<sub>3,5K</sub>-G3-PEG<sub>600</sub>-BOC was dissolved in a 1:1 mixture of dichloromethane and trifluoroacetic acid (2 mL of total volume) and stirred for 30 min at room temperature. The solvent was then completely removed by rotary evaporation, and the purified product was redissolved in dimethyl sulfoxide (DMSO) (3 mL). After dialysis for 24 h and lyophilization for 2 days, the final product of PCL<sub>3,5K</sub>-G3-PEG<sub>600</sub>-NH<sub>2</sub> was obtained.

The acetylation and carboxylation reactions were conducted according to our published protocol.<sup>19</sup> Briefly, for acetylation, PCL<sub>3,5K</sub>-G3-PEG<sub>600</sub>-NH<sub>2</sub> (30 mg, 0.004 mmol) was dissolved in DMSO (2 mL) containing TEA (38 mg, 0.376 mmol). Acetic anhydride (31.95 mg, 0.313 mmol) was then added dropwise to the stirring solution. For carboxylation, PCL<sub>3,5K</sub>-G3-PEG<sub>600</sub>-NH<sub>2</sub> (30 mg, 0.004 mmol) was dissolved in DMSO (2 mL) containing pyridine (12.3 mg, 0.156 mmol) to which a DMSO solution (1 mL) of succinic anhydride (15.7 mg, 0.156 mmol) was added dropwise with vigorous stirring. Both reactions were carried out at room temperature for 24 h. After dialysis for 24 h and lyophilization for 2 days, PCL<sub>3,5K</sub>-G3-PEG<sub>600</sub>-Ac and PCL<sub>3,5K</sub>-G3-PEG<sub>600</sub>-COOH were obtained as powder.

To prepare rhodamine-labeled PDC<sub>600</sub>, PCL<sub>3,5K</sub>-G3-PEG<sub>600</sub>-NH<sub>2</sub> (30 mg, 0.004 mmol) was dissolved in DMSO (2 mL) to which an NHS-rhodamine (5.16 mg, 0.0098 mmol) solution in DMSO (1 mL) was subsequently added dropwise. The reaction was carried out at room temperature for 24 h. The remaining primary amine groups were then acetylated by addition of acetic anhydride (31.95 mg, 0.313 mmol) in the presence of TEA (38 mg, 0.376 mmol), followed by stirring for an additional 24 h at room temperature. The reaction mixture was dialyzed against water for 48 h to remove unreacted

rhodamine followed by 2 days of lyophilization, resulting in the final product of PDC<sub>600</sub>-Rhod. The same method was employed to synthesize PDC<sub>2K</sub>-Rhod and linear PCL<sub>3,5K</sub>-PEG<sub>2K</sub>-Rhod (LBC<sub>2K</sub>-Rhod).

In addition, G4 PAMAM dendrimers, used as control in this study, were purified using repetitive dialysis and lyophilization as described earlier,<sup>20</sup> followed by conjugation with rhodamine, using EDC/NHS chemistry, resulting in G4-NH<sub>2</sub>-Rhod.<sup>20,21</sup>

**Micelle Preparation.** To prepare blank micelles, each PDC (PDC<sub>600</sub>-NH<sub>2</sub>, PDC<sub>600</sub>-COOH, or PDC<sub>600</sub>-Ac) (5 mg) or linear block copolymer (LBC, PCL<sub>3,5K</sub>-PEG<sub>2K</sub>) that was synthesized in our laboratory as described earlier<sup>18</sup> was first dissolved in DMF (2 mL), vortexed vigorously for 5 min, and stirred for 10 min until it was completely dissolved. dH<sub>2</sub>O (1.8 mL) was then added dropwise into each of the DMF solutions under stirring. Each solution was dialyzed against dH<sub>2</sub>O (4 L) in a dialysis membrane (3.5 kg/mol MWCO) at room temperature for 24 h, followed by centrifugation at 9300 × g for 5 min to remove large aggregates. The supernatants containing the resulting micelles were collected and immediately used for subsequent experiments.

The rhodamine-labeled micelles, dual-dye micelles, and Förster resonance energy transfer (FRET) micelles were prepared using the same method described above except for the inclusion of rhodamine-labeled polymer or hydrophobic dyes in polymer solution. For rhodamine-labeled micelles, PDC-Rhod (0.5 mg, 10 wt %) was mixed with each PDC solution in DMF. For dual dye micelles, PDC<sub>600</sub>-Rhod or LBC<sub>2K</sub>-Rhod (0.5 mg, 10 wt %) was incorporated into each polymer solution in DMF, along with 3,3'-dioctadecyloxycarbocyanine perchlorate (DiO, 25 μg, 0.5 wt %). Finally, for FRET micelles, DiO (25 μg, 0.5 wt %) and 1,1'-dioctadecyl-3,3,3',3'-tetramethylindocarbocyanine perchlorate (DiI, 25 μg, 0.5 wt %) were added into PDC<sub>600</sub>-Ac or PCL<sub>3,5K</sub>-PEG<sub>2K</sub> in DMF.

**Dynamic Light Scattering and Zeta-Potential Analysis.** Particle size of the various DMs (1 mg/mL) was measured using a NICOMP 380 zeta potential/particle sizer (Particle Sizing Systems, Santa Barbara, CA). All measurements were performed in triplicate in double distilled water using unfiltered micelle samples.

**Transmission Electron Microscopy.** The morphology of each DM was visualized using transmission electron microscopy (TEM, JEM-1220, JEOL Ltd., Japan). A drop (5 μL) of each micellar suspension (0.2 mg/mL) was placed on a 300 mesh copper grid coated with carbon (Electron Microscopy Sciences, Hatfield, PA). All samples were stained with a drop (5 μL) of 2% phosphotungstic acid (pH 7) and dried in a desiccator at room temperature for 1 day before observed using TEM as described earlier.<sup>19</sup>

**Confocal Laser Scanning Microscopy.** KB cells were seeded in glass bottom culture dishes at a density of 1 or 4 × 10<sup>5</sup> cells/well on 8-well Millicell EZ slides (Millipore Corporation, Billerica, MA) or glass-bottomed Petri dishes (MatTek Corporation, Ashland, MA) and incubated for 24 h. Cells were then treated with rhodamine-labeled DM<sub>600</sub> (8 μM), rhodamine-labeled DM<sub>2K</sub> (4 μM), rhodamine-labeled G4 PAMAM dendrimer (1 μM), or free rhodamine (0.2 μM) all in PBS for 2 or 4 h. The concentrations of all samples were adjusted to normalize the amounts of rhodamine using fluorescent spectroscopy prior to the experiment. For DiO-loaded, rhodamine-labeled (dual-dye) micelles, KB cells were seeded in glass bottom culture dishes using the protocol described above, and cells were treated with dual-dye DM<sub>600</sub> (60 μg/mL) or dual-dye LBC(PCL<sub>3,5K</sub>-PEG<sub>2K</sub>)-based micelles (60 μg/mL) in RPMI without supplements for 4, 8, 24, or 48 h. After incubation, the cells were washed twice using PBS and fixed using a 4% paraformaldehyde solution. When the nuclear staining was needed, a mounting agent containing DAPI (Vectashield H-1200, Vector Laboratories, Inc., Burlingame, CA) was used after fixation. The fixed cells were visualized by a Carl Zeiss confocal microscope (LSM 710, Carl Zeiss MicroImaging GmbH, Gena, Germany) using a diode laser (405 nm) for DAPI, an argon laser (488 nm) for DiO, and a DPSS laser (561 nm) for rhodamine. A 40× objective (Objective "C-Apochromat" 40x/1,20 W corr, Carl Zeiss MicroImaging GmbH, Gena, Germany) was used. All obtained images were processed using Zen software (Carl Zeiss MicroImaging GmbH, Gena, Germany).

**Flow Cytometry Analysis.** KB cells were seeded in 12-well plates at a density of  $2 \times 10^5$  cells/well and incubated for 24 h. Cells were then treated with rhodamine-labeled DM<sub>600</sub> (8  $\mu$ M), rhodamine-labeled DM<sub>2K</sub> (4  $\mu$ M), rhodamine-labeled G4 PAMAM dendrimer (1  $\mu$ M), or free rhodamine (0.2  $\mu$ M), all in PBS, for 2 h. For dual-dye micelles, cells were treated with dual-dye DM<sub>600</sub> (60  $\mu$ g/mL) or dual-dye LBC (PCL<sub>3,5K</sub>-PEG<sub>2K</sub>)-based micelles (60  $\mu$ g/mL) in RPMI without supplements for 4, 8, 24, or 48 h. The treated cells were washed twice with PBS and suspended by addition of trypsin/EDTA. The cell suspensions were centrifuged at  $228 \times g$  for 5 min, and the supernatants were discarded. The resulting cell pellets were resuspended in a paraformaldehyde solution (1% w/v, 500  $\mu$ L) and transferred to flow cytometry sample tubes. The samples were examined using a LSR Fortessa flow cytometer (Becton Dickinson, Franklin Lakes, NJ) as described earlier.<sup>19</sup>

**MTS Assay.** KB cells were seeded in 96-well plates at a density of  $1 \times 10^4$  cells/well and grown in RPMI media for 24 h. Cells were then treated with various DMs and G4 PAMAM dendrimers at various concentrations ranging from 1 to 100  $\mu$ M. After 24 h, the cells were washed twice with PBS. Cell viability was assessed using a CellTiter 96 Aqueous One Solution (MTS) Assay (Promega, Madison, WI) according to the manufacturer's protocol. The UV absorbance was measured at 490 nm using a Labsystems Multiskan Plus microplate reader (Labsystems, Finland). Mean cell viabilities were determined relative to a negative control (untreated cells) and a positive control (cells lysed using 0.1% Triton-X) ( $n = 5$ ).

**FRET Spectroscopy.** FRET-DM<sub>600</sub>-Ac micelles (60  $\mu$ g/mL) or FRET-LBC (PCL<sub>3,5K</sub>-PEG<sub>2K</sub>)-based micelles (60  $\mu$ g/mL) were incubated in PBS at 37 °C for up to 48 h. Fluorescence intensities were measured using a spectrofluorometer (RF 1501, Shimadzu, Japan) by scanning the emission spectra from 495 to 600 nm at an excitation wavelength of 484 nm. FRET ratios were calculated as  $I_{565}/(I_{565} + I_{501})$ .<sup>22</sup>

**Atomistic Molecular Dynamics (MD) Simulation.** The MD simulations were performed with NAMD<sup>23</sup> and the CHARMM force field (CHARMM27, C35r revision for ethers and general force field).<sup>24,25</sup> Nonbonding interactions were calculated using a cutoff distance of  $d = 10$  Å, and long-range electrostatic interactions were calculated by the PME method.<sup>26</sup> The systems were simulated in the NPT ensemble, using the Langevin dynamics with a damping constant of  $\gamma_{\text{Lang}} = 0.1$  p/s, and the time step of 2 fs. The micelles were prepared from  $N_{\text{agg}} = 15$  individual copolymers (unimers) of PDC-NH<sub>3</sub><sup>+</sup> with two different PEG chain lengths of molecular weight 600 and 2000 g/mol. Initially, the unimers were spherically distributed to form the basic micelle structure and compacted by brief simulations in vacuum. The micelles were then simulated alone in ionic solutions for 10 ns at  $T = 300$  K and  $P = 1$  bar. We also used CHARMM-GUI (a Web-based graphical user interface for CHARMM)<sup>27,28</sup> to prepare a biological membrane consisting of two different types of lipid molecules. The dipalmitoylphosphatidylcholine (DMPC) and dipalmitoylphosphatidylglycerol (DMPG) lipid molecules were used in a 3:1 ratio. Similar to the condition used for the micelles, the membrane (size 230 Å  $\times$  230 Å) was equilibrated for 2 ns ( $\gamma_{\text{Lang}} = 1.0$  p/s) using the CHARMM36 lipid force field. After equilibrium, both micelles were placed 5 Å above the membrane, and the whole systems were placed in an ionic solution with a salt concentration of 150 mM (physiological salt concentration). First, the systems were equilibrated for 5 ns while keeping the micelle and membrane atoms fixed. Then, all the atoms were released, and the simulations were continued for 75 ns ( $\gamma_{\text{Lang}} = 0.1$  p/s). We continued the micelle simulation without membrane for 30 ns to find out the effect of the negatively charged membrane on the morphology of positively charged micelle. The Coulombic potential energy was calculated from eq 1

$$U(r) = \frac{1}{4\pi\epsilon\epsilon_0} \sum_{i=1}^{120} \sum_{j=1}^{640} \frac{q_i q_j}{r_{ij}} \quad (1)$$

where  $U(r)$  is Coulombic potential energy,  $\epsilon$  is the dielectric constant of water,  $\epsilon_0$  is the vacuum permittivity,  $i$  is the number of positively charged point at the surface of the micelle,  $j$  is the number of

negatively charged point at the upper layer of the lipid bilayer, and  $r_{ij}$  is the distance between the positive and negative charge ( $q_i = -q_j = 1.6 \times 10^{-19}$  C,  $\epsilon = 80$ , and  $\epsilon_0 = 8.8542 \times 10^{-12}$  C<sup>2</sup> N<sup>-1</sup> m<sup>-2</sup>).

## RESULTS AND DISCUSSION

**Preparation of End-Group-Modified DMs.** End-group-modified PDCs were synthesized using a modified version of our previously published protocol.<sup>19</sup> Briefly, alkyne-core-functionalized polyester G3 dendron (870 g/mol) was conjugated with azido-functionalized PCL (3500 g/mol) using click chemistry, followed by PEGylation of the dendritic arms using heterobifunctional NH<sub>2</sub>-PEG<sub>600</sub>-BOC. The end groups of the PDCs were then modified to amine (PDC<sub>600</sub>-NH<sub>2</sub>), carboxylate (PDC<sub>600</sub>-COOH), and acetamide groups (PDC<sub>600</sub>-Ac), followed by extensive characterization using <sup>1</sup>H NMR and GPC (Table 1 and Figure S1 of the Supporting

**Table 1. Molecular Weights and Polydispersity Indices (PDIs) of PDCs**

polymer	theor $M_w$	$M_n$ (NMR) <sup>a</sup>	$M_n$ (GPC) <sup>b</sup>	PDI <sup>c</sup>
PCL <sub>3,5K</sub> -G3-PEG <sub>600</sub> -NH <sub>2</sub>	9297	7075	— <sup>d</sup>	— <sup>d</sup>
PCL <sub>3,5K</sub> -G3-PEG <sub>600</sub> -Ac	9505	7313	8020	1.052
PCL <sub>3,5K</sub> -G3-PEG <sub>600</sub> -COOH	9521	7568	7998	1.303
PCL <sub>3,5K</sub> -G3-PEG <sub>600</sub> -Rhod	9755	6839	7538	1.164

<sup>a</sup>Number-averaged molecular weight,  $M_n$ , estimated by <sup>1</sup>H NMR. <sup>b</sup>Measured by GPC using  $d_n/d_c$  values. <sup>c</sup>Calculated by weight-average molecular weights divided by number-average molecular weights using the data obtained by GPC. <sup>d</sup>Not measured due to the limited solubility of amine-terminated PDC in THF.

Information). Full chemical characterization of PDC is presented previously.<sup>18</sup> Briefly, the characteristic peaks of polyester dendron were observed at 4.40–4.18 and 1.22–1.15 ppm. The repeating unit of PCL appeared at 4.06, 2.30, 1.62, and 1.35 ppm, and the repeating unit of PEG appeared at 3.62 ppm. Also, the characteristic peaks of terminal groups appeared at 3.13 ppm for PDC<sub>600</sub>-NH<sub>2</sub>, 1.96 ppm for PDC<sub>600</sub>-Ac, and 2.52 and 2.62 ppm for PDC<sub>600</sub>-COOH. To employ fluorescence-based analytical techniques, rhodamine-conjugated PDC<sub>600</sub> (PDC<sub>600</sub>-Rhod) was also prepared and characterized. DMs were prepared by self-assembly of the end-group-modified PDCs using the dialysis method.<sup>18</sup> Figure 1A depicts the structure of a DM assembled from amine-terminated PDCs as an example. The particle size distributions, zeta-potentials, and CMCs of all three end-group-modified DMs, along with DM<sub>2K</sub>-NH<sub>2</sub> included as a control, are listed in Table 2. The hydrodynamic diameters of DM<sub>600</sub>-NH<sub>2</sub>, DM<sub>600</sub>-Ac, and DM<sub>600</sub>-COOH were measured to be approximately 47, 23, and 47 nm, respectively, which was consistent with our previous findings where DM<sub>2K</sub>-NH<sub>2</sub> and DM<sub>2K</sub>-COOH were larger than DM<sub>2K</sub>-Ac.<sup>19</sup> The zeta-potential measurements confirmed the surface modification, where DM<sub>600</sub>-COOH and DM<sub>600</sub>-Ac were measured at  $-21$  and  $0$  mV, respectively, which was significantly different from  $+30$  mV of DM<sub>600</sub>-NH<sub>2</sub>. The CMCs of the three PDCs were consistent with our previously measured values (on the order of  $10^{-7}$  M) of PDCs with 2K PEG (PDC<sub>2K</sub>) as well as that of LMs ( $2.4 \times 10^{-7}$  M).<sup>18,19</sup> Transmission electron microscopy (TEM) images (Figure S2) revealed that all DM<sub>600</sub> were spherical with sizes similar to those of DM<sub>2K</sub>.<sup>19</sup> Interestingly, the core size of the both DM<sub>600</sub> and DM<sub>2K</sub> were similar, even though the PDC<sub>600</sub> has a lower HLB (16.56 for PDC<sub>2K</sub> and 12.37 for PDC<sub>600</sub>), which

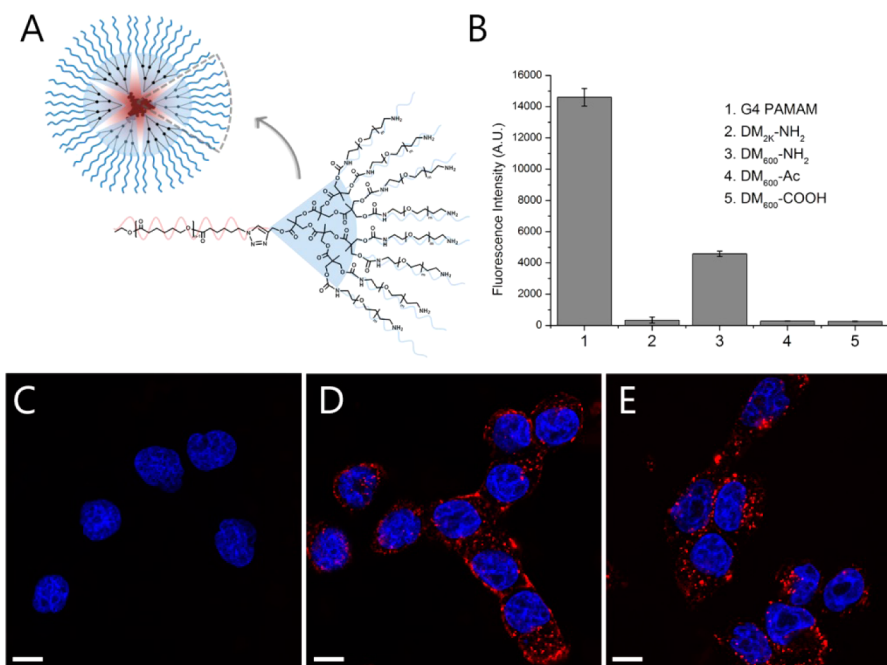


**Figure 1.** Cellular interactions of end-group-modified DMs and G4 PAMAM dendrimers. (A) Schematic diagram and chemical structure of DM and PDC-NH<sub>2</sub>. (B) Flow cytometry results of the cell association of end-group-modified DMs and G4 PAMAM dendrimers after 2 h of incubation. Confocal images of KB cells treated with (C) rhodamine-labeled DM<sub>2K</sub>-NH<sub>2</sub>, (D) DM<sub>600</sub>-NH<sub>2</sub>, and (E) G4 PAMAM at 37 °C for 2 h. Nuclei were stained using DAPI (blue color). Scale bar: 10 μm. Note that both amine-terminated DM<sub>600</sub>-NH<sub>2</sub> (D) and PAMAM dendrimers (E) exhibit significant cell interactions as opposed to DM<sub>2K</sub>-NH<sub>2</sub> (C), DM<sub>600</sub>-Ac, and DM<sub>600</sub>-COOH, indicating that the role of the surface charge and PEG chain length on cell interactions of DMs.

**Table 2. Characterization of End-Group-Modified Dendron Micelles**

micelles	particle size (nm)	zeta-potential (mV)	CMC (10 <sup>-7</sup> M)
DM <sub>600</sub> -NH <sub>2</sub>	47.0 ± 7.9	29.58 ± 1.56	4.7
DM <sub>600</sub> -Ac	22.5 ± 9.6	-0.37 ± 0.71	2.9
DM <sub>600</sub> -COOH	47.2 ± 9.2	-21.22 ± 4.02	3.5
DM <sub>2K</sub> -NH <sub>2</sub>	52.8 ± 7.0 <sup>a</sup>	20.75 ± 1.76	9.3 <sup>a</sup>

<sup>a</sup>Measured previously.<sup>19</sup>

suggested an increased copolymer aggregation number ( $N_{agg}$ ) for DM<sub>600</sub>.<sup>29,30</sup> Collectively, these data demonstrate that the end-group-modified PDCs were successfully prepared and formed DMs with various surface groups.

#### Cellular Interactions of the Surface-Modified Micelles.

The end-group effect of DMs with shorter PEG chains on their cell interactions was first evaluated in terms of cellular uptake and cytotoxicity. After incubation with KB cells, the *in vitro* behaviors of DM<sub>600</sub> with -NH<sub>2</sub>, -COOH, and -Ac terminal groups, DM<sub>2K</sub>-NH<sub>2</sub>, and G4 PAMAM dendrimers (G4-NH<sub>2</sub>) were observed using confocal microscopy and flow cytometry, as shown in Figure 1B–E. PDC<sub>600</sub>-Rhod was incorporated at 10% (w/w) of each DM<sub>600</sub> for fluorescence-based detection. No significant cellular interactions were observed for charge neutral DM<sub>600</sub>-Ac and negatively charged DM<sub>600</sub>-COOH. The positive control G4-NH<sub>2</sub> exhibited a strong, charge-dependent interaction as expected. As we reported earlier,<sup>19</sup> DM<sub>2K</sub>-NH<sub>2</sub>, despite their positively charged surfaces, did not show any noticeable cellular interactions. Markedly, DM<sub>600</sub>-NH<sub>2</sub> displayed a significant cellular interaction, which proved our hypothesis that shortening the PEG chain length would enhance the end-group effect of DMs, converting previously observed charge-independent interactions to be charge-depend-

ent. We verified this result using the MCF-7 cell line as well (Figure S3), which confirmed that the observed charge-dependent cell interactions of DM<sub>600</sub> were not cell specific.

The charge-dependent cytotoxicity profiles of DM<sub>600</sub> were also evaluated using an MTS assay (Figure 2). Unlike DM<sub>2K</sub>-NH<sub>2</sub>, DM<sub>600</sub>-Ac, and DM<sub>600</sub>-COOH that all exhibited no apparent cytotoxicity, DM<sub>600</sub>-NH<sub>2</sub> displayed moderate cytotoxicity at 100 μM. However, the cytotoxicity of DM<sub>600</sub>-NH<sub>2</sub>

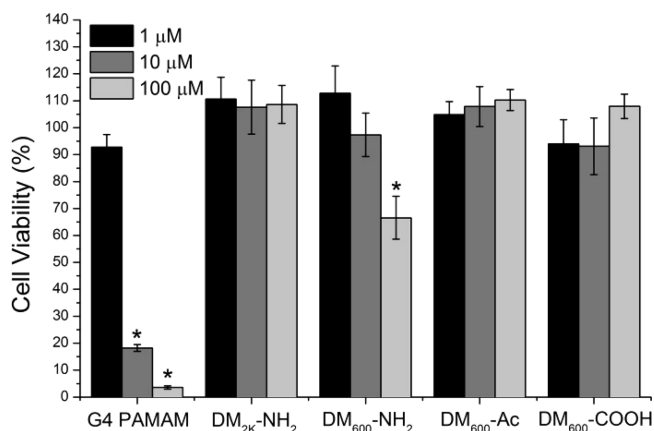


**Figure 2.** Cell viability of KB cells after treated with end-group-modified DMs and G4 PAMAM dendrimers at concentrations of 1–100 μM for 24 h, as measured using MTS assay. Amine-terminated PAMAM dendrimers induce significant cytotoxicity, and DM<sub>600</sub>-NH<sub>2</sub> induced a modest level of cytotoxicity only at a high concentration. All other micelles that do not show cell interactions do not cause any noticeable cell death. Data are normalized relative to a negative control (untreated cells). Results are presented as average ± SD ( $n = 5$ ). \* $p < 0.05$  compared to the negative control.

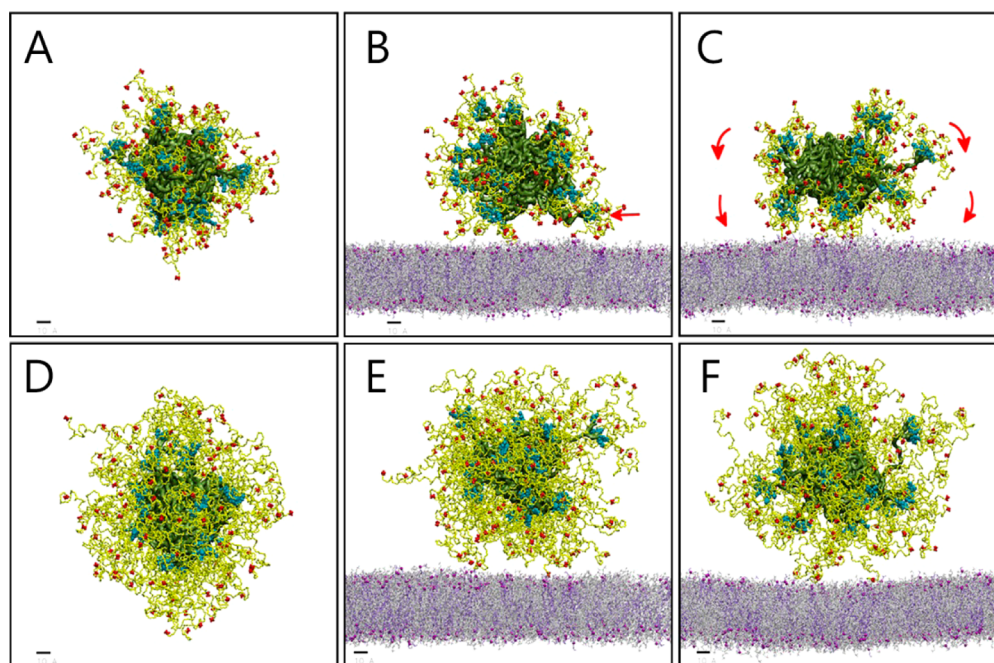


**Figure 3.** Atomistic MD simulations of (A–C)  $\text{DM}_{600}\text{-NH}_3^+$  and (D–F)  $\text{DM}_{2K}\text{-NH}_3^+$  in an ionic solution (150 mM NaCl) with and without lipid membranes. The core and the dendrons are visualized in dark green. The functionalized PEG chains are shown in atomistic details with the amine termini highlighted in red. (A, D) show the micelles in solution; (B, C, E, F) show the micelles placed on lipid membranes for 30 ns (B, E) and 75 ns (C, F). Arrows indicate the stretching and deformation of  $\text{DM}_{600}\text{-NH}_3^+$  upon interaction with the lipid membrane. Scale bar: 1 nm.

appeared to be significantly smaller than that of  $\text{G4-NH}_2$ , probably due to its 5-fold higher molecular-weight-to-surface-charge ratio than  $\text{G4-NH}_2$ . These cell uptake and cytotoxicity results indicate that the length of the PEG corona modulates the charge-dependent cellular interactions of DMs.

**Molecular Dynamics (MD) Simulation.** To better understand these observations, we conducted atomistic molecular dynamics (MD) simulations of the experimental systems. Figures 3A and 3D show the conformation of  $\text{DM}_{600}\text{-NH}_3^+$  and  $\text{DM}_{2K}\text{-NH}_3^+$  in 150 mM NaCl solution after 30 ns equilibration.<sup>31</sup> Both micelles were stable, as determined by the maintenance of their integrity and spherical shape. We also modeled a biological membrane in the same solution, using dipalmitoylphosphatidylcholine (neutral) and dipalmitoylphosphatidylglycerol (negatively charged) lipid molecules in a 3:1 ratio. Then we placed both DMs within 5 Å of the membrane and simulated the whole system.<sup>32</sup> Over the course of 75 ns simulations, significant differences in the behavior of the two DMs were observed. After 30 ns of equilibration, individual PDCs were pulled away from the core of  $\text{DM}_{600}\text{-NH}_3^+$  and drawn toward the membrane surface, due to strong Coulombic attraction, as shown in Figure 3B. After 60 ns,  $\text{DM}_{600}\text{-NH}_3^+$  began to flatten and spread over the membrane surface, and at 75 ns it formed a pancake-like shape (Figure 3C). This behavior can be understood as a consequence of a “coherent” binding of the terminal amine groups of PDCs to the negatively charged membrane. The short PEG chains provide direct links between the  $-\text{NH}_3^+$  groups and the dendron holding them, which means that several  $-\text{NH}_3^+$  groups attached to the same dendron can act in a concerted way (like a polyion) in the presence of charged membrane pulling them by Coulombic coupling to the membrane. On the other hand,  $\text{DM}_{2K}\text{-NH}_3^+$  stably settled on the membrane but did not display any noticeable conformational changes (Figure 3E,F). The Coulombic binding energies between DMs and the

membrane were calculated with our code (no ions considered) and found to be 17% higher for  $\text{DM}_{600}\text{-NH}_3^+$  than  $\text{DM}_{2K}\text{-NH}_3^+$  ( $0.224 \times 10^{-16}$  J vs  $0.189 \times 10^{-16}$  J). These results were in agreement with our *in vitro* observations of the  $\text{DM}_{600}\text{-NH}_3^+$  cell insertion (stronger interactions with the membrane).

Next, we analyzed further the mechanism of PEG chain-length-dependent cellular interactions of DMs. Our previous study suggested that the lack of cellular interactions of  $\text{DM}_{2K}\text{-NH}_2$  was in part due to the back-folding of the amine termini into the PEG layers, impeding the cellular interactions.<sup>19</sup> We calculated the number of oxygen atoms in the PEG chains present within a distance of 2.5 Å from the terminal amine hydrogens of  $\text{DM}_{600}\text{-NH}_3^+$  by averaging the results over 300 frames (1.2 ns of equilibration) to quantitate the number of intramolecular hydrogen bonds that can be formed. The average numbers of oxygen atoms were  $165 \pm 8.9$  and  $212 \pm 8.6$  per frame for  $\text{DM}_{600}\text{-NH}_3^+$  and  $\text{DM}_{2K}\text{-NH}_3^+$ , respectively. A lower number of oxygen atoms that are available for hydrogen bond formation would indicate less sequestration of the amine termini by PEG chains, thus increasing the exposure of amine groups at the  $\text{DM}_{600}\text{-NH}_3^+$  surface. This phenomenon was also supported by the zeta-potential measurements of  $\text{DM}_{600}\text{-NH}_2$  and  $\text{DM}_{2K}\text{-NH}_2$ , as summarized in Table 2. The higher surface exposure of the amine termini on  $\text{DM}_{600}\text{-NH}_2$  resulted in a higher zeta-potential value ( $\sim 30$  mV) compared to that ( $\sim 21$  mV) of  $\text{DM}_{2K}\text{-NH}_2$ . Taken together, these results revealed that charge-dependent end-group effect of DMs could be pronounced or sequestered by the number of hydrogen bonds formed between the PEG backbone and the amine termini.

The increased cellular interactions of  $\text{DM}_{600}\text{-NH}_2$  can be also explained by the intrinsic properties of the corresponding PDCs. The charge-number-to-molecular-weight ratio is approximately 2-fold higher for  $\text{PDC}_{600}$  than  $\text{PDC}_{2K}$ , which accentuates the end-group effect of the DMs. Furthermore,

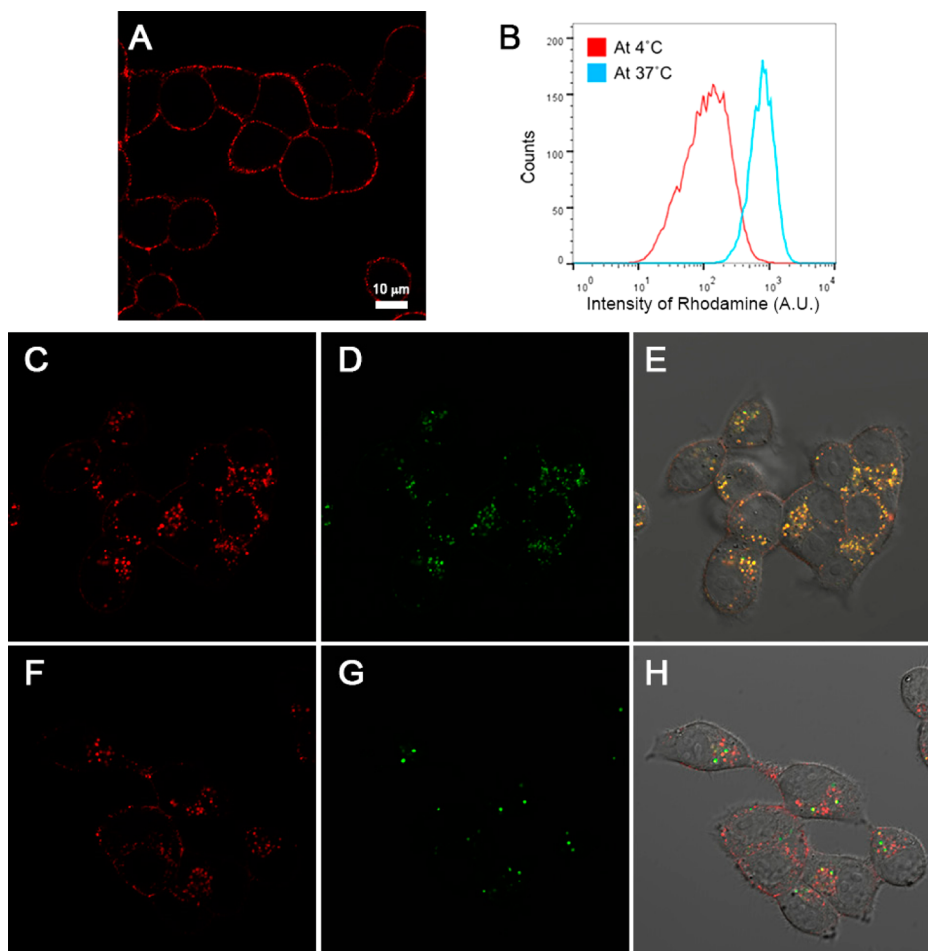


**Figure 4.** Cell internalization mechanism of  $DM_{600}\text{-NH}_2$ . (A) KB cells treated with rhodamine-labeled  $DM_{600}\text{-NH}_2$  at 4 °C for 2 h. (B) Flow cytometry histograms representing the cell association of  $DM_{600}\text{-NH}_2$  at and 37 °C. The lack of internalization and the significantly reduced cell association at 4 °C indicate that  $DM_{600}\text{-NH}_2$  internalizes into KB cells in an energy-dependent manner. (C–E) KB cells treated with dual-dye  $DM_{600}\text{-NH}_2$  at 37 °C for 4 h. (F–H) KB cells treated with the mixture of free DiO and rhodamine-labeled  $DM_{600}\text{-NH}_2$  at 37 °C for 4 h. (C, F: red channel for rhodamine; D, G: green channel for DiO; E, H: merged images) The correlation (Pearson's) coefficients between red and green signals are 0.939 and 0.317 in (E) and (H), respectively. The colocalization of the two signals shown in (E) confirms that  $DM_{600}\text{-NH}_2$  internalizes into the cells together with the encapsulated dye. Scale bar: 10  $\mu\text{m}$ .

shorter PEG chains lead to a decreased HLB of the copolymer, resulting in a higher  $N_{\text{agg}}$  of micelles.<sup>30</sup> A DM with a higher  $N_{\text{agg}}$  contains more PDCs, and thus more terminal groups are expected to be present on its surface. The lower the number of intramolecular hydrogen bonds, the higher the charge-number-to-molecular-weight ratio and the greater  $N_{\text{agg}}$ , which all contribute to the increased cellular interactions of  $DM_{600}\text{-NH}_2$  and a more pronounced end-group effect compared to  $DM_{2K}\text{-NH}_2$ .

**Energy-Dependent Internalization of  $DM_{600}\text{-NH}_2$ .** Low-generation PAMAM dendrimers (generations 2–5) (~2–6 nm) have been reported to internalize into cells via energy-dependent endocytosis.<sup>10,14,33–35</sup> On the other hand, in addition to energy-dependent mechanisms, energy-independent mechanisms such as nanoscale hole formation have been proposed for larger G7 PAMAM (~10 nm) dendrimers.<sup>17</sup> The nanoscale hole formation causes cytoplasm leakage and is usually accompanied by higher cytotoxicity. Since the end groups of DMs are coordinated by G3 dendrons and the self-assembled structures are much larger than G7 dendrimers, we sought to determine which dendrimer internalization mechanism governs cell entry of  $DM_{600}\text{-NH}_2$ .

The cellular uptake studies were carried out at 4 °C to investigate whether the nonspecific charge-dependent cell interactions of  $DM_{600}\text{-NH}_2$  were energy-dependent. Figure 4A shows that  $DM_{600}\text{-NH}_2$  was mostly observed on the cell surface without significant cell entry, indicating that their uptake was primarily energy-dependent. Additionally, flow cytometry analysis (Figure 4B) revealed that the cell association of  $DM_{600}\text{-NH}_2$  at 4 °C was only 25% of that at 37 °C. We then concluded that the cellular internalization mechanism of  $DM_{600}\text{-NH}_2$  was similar to that of low-generation PAMAM dendrimers, which was in good agreement with their moderate cytotoxicity shown earlier. However, further investigation is obviously required to fully understand the uptake mechanism of  $DM_{600}\text{-NH}_2$ .

**Cellular Uptake of DiO-Loaded, Rhodamine-Labeled (Dual-Dye) Micelles.** The MD simulation results demonstrated that the nonspecific membrane interactions may likely result in a partial pulling of individual PDCs from  $DM_{600}\text{-NH}_2$ , followed by its large-scale deformations, causing the destabilization of the micelle structure following the cell membrane interaction. Since this may deteriorate the therapeutic effect when DMs are used as drug carriers, we examined the integrity

of  $\text{DM}_{600}\text{-NH}_2$  upon cell internalization. To investigate this, we prepared a dual-dye DM system by encapsulating DiO into rhodamine-labeled  $\text{DM}_{600}\text{-NH}_2$ , which enabled colocalization studies using confocal microscopy. As shown in Figure 4C–E, red fluorescence (rhodamine) and green signals (DiO) were overlapped inside the KB cells after treatment with  $\text{DM}_{600}\text{-NH}_2$  at 37 °C for 4 h. A colocalization analysis of the red and green signals was then performed using ImageJ.<sup>36</sup> The Pearson's coefficient of these two colors was 0.939, which indicated almost complete colocalization of  $\text{DM}_{600}\text{-NH}_2$  with DiO. To exclude the possibility that DiO was released extracellularly and then cointernalized into cells along with rhodamine-labeled DMs, KB cells were also treated with a mixture of DiO and rhodamine-labeled  $\text{DM}_{600}\text{-NH}_2$ . The poor correlation (Pearson's coefficient: 0.317) between the two signals as shown in Figure 4F–H confirmed that extracellularly released DiO was not cointernalized into cells with  $\text{DM}_{600}\text{-NH}_2$ . These results demonstrated that  $\text{DM}_{600}\text{-NH}_2$  maintained its structural integrity during its nonspecific interaction with the cell membrane and carried the hydrophobic cargo into the cells.

One of the major rationales behind our DM design was to take advantage of the dendritic structure to achieve enhanced structural stability over conventional LBC-based systems owing to its preorganized conical molecular architecture and ability to accommodate a significantly denser outer PEG layer. To test this hypothesis, we compared dual-dye DMs with LMs in terms of their ability to prevent premature release of hydrophobic cargos. KB cells were incubated and monitored after treatment with dual-dye  $\text{DM}_{600}\text{-Ac}$  and LMs made from  $\text{PCL}_{3.5\text{K}}\text{-PEG}_{2\text{K}}\text{-OMe}$ . Note that we used charge neutral micelles to inhibit their nonspecific cell entry based on electrostatic interactions. As shown in Figure 5A,B and Figure S4, the lack of a rhodamine signal indicated that neither  $\text{DM}_{600}\text{-Ac}$  nor LMs were internalized into the cells even after 48 h of incubation. Interestingly, a negligible uptake of DiO was observed from KB cells treated with  $\text{DM}_{600}\text{-Ac}$ , whereas a significantly stronger DiO signal was observed for cells treated with LMs. Flow cytometry analysis shown in Figure 5C further supported that the cell-associated DiO signal was higher for the cells incubated with LMs than those with  $\text{DM}_{600}\text{-Ac}$ . These results are in agreement with a previous report where hydrophobic probes such as DiO that were encapsulated into LMs composed of PCL–PEG or polylactide–PEG were released from the micelles extracellularly.<sup>37</sup> Because the both micelles showed a great degree of thermodynamic stability (low CMCs) and maintained structural integrity at the testing concentration (60  $\mu\text{g}/\text{mL}$ ) as measured by FRET (Figure S5),<sup>22</sup> this uncontrolled release was attributed to the hydrophobic cell membranes extracting the hydrophobic cargos from the micelle cores. Our results herein indicate the superior stability of DMs over LMs for hydrophobic drug delivery. Despite the similar CMC values of DMs and LMs, the dendritic architecture, in combination of the dense PEG layers of DMs, likely allowed enhanced protection of the encapsulated hydrophobic cargo molecules compared to LMs. This enhanced stability is particularly important for the future development of targeted NPs to minimize premature drug release and ultimately improve therapeutic efficacy.

## CONCLUSIONS

Here we report that the length of hydrophilic PEG chains can control the charged end-group effect of DMs. With the short PEG chains (600 g/mol), positively charged  $\text{DM}_{600}\text{-NH}_2$

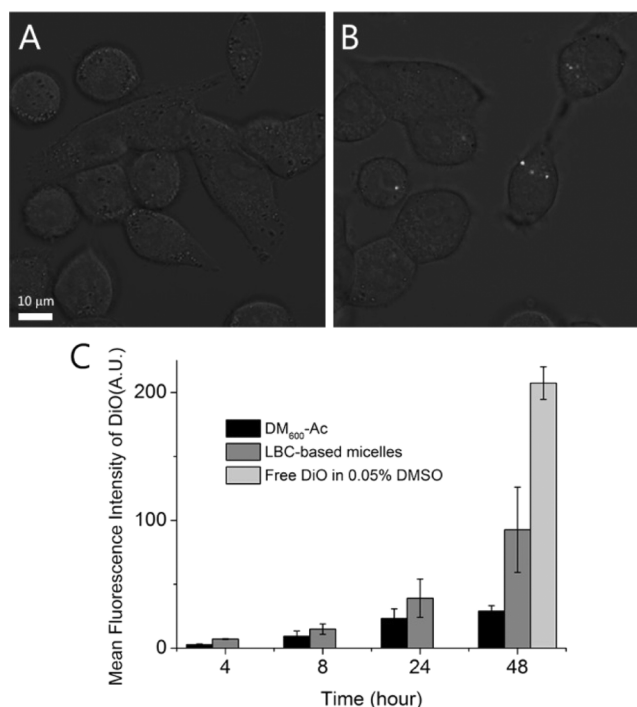


**Figure 5.** Confocal images of KB cells treated with dual-dye (A)  $\text{DM}_{600}\text{-Ac}$  and (B) LBC ( $\text{PCL}_{3.5\text{K}}\text{-PEG}_{2\text{K}}$ )-based micelles at 37 °C for 4 h. Images A and B are merged images of red (rhodamine) and green (DiO) channels along with differential interference contrast (DIC) images. (C) Flow cytometry data of the cellular association of  $\text{DM}_{600}\text{-Ac}$ , LBC-based micelles, and free DiO in 0.05% DMSO at various time points. Scale bar: 10  $\mu\text{m}$ . A significantly lower extracellular release of the encapsulated DiO was observed in  $\text{DM}_{600}\text{-Ac}$  compared to LBC-based micelles, indicating the enhanced stability of the encapsulated dye in DMs.

showed charge-dependent nonspecific cellular interactions and modest cytotoxicity, whereas the DMs prepared from longer PEG chains (2000 g/mol),  $\text{DM}_{2\text{K}}\text{-NH}_2$ , did not. This result was further supported by the MD data, where  $\text{DM}_{600}\text{-NH}_2$  exhibited less hydrogen bonding formation than  $\text{DM}_{2\text{K}}\text{-NH}_2$ , thereby pronouncing the surface charge effect. Surface modification of  $\text{DM}_{600}$  to charge neutral or negatively charged groups substantially decreased the charge-based cell interactions. In addition, we found that  $\text{DM}_{600}\text{-NH}_2$  maintained its structural integrity after binding to KB cell membranes and internalized through an energy-dependent pathway. No DMs display any noticeable leakage of an encapsulated dye, whereas the LM allowed a degree of dye leakage, indicating that the dense, dendritic PEG corona enhanced the encapsulation stability of DMs. Our results integrating both *in vitro* and MD simulation data support the potential to use DMs as a drug delivery platform of which cellular interactions can be facily modulated by surface functionalization and the PEG chain length. This study helps to understand the role of surface charge, PEG corona, and polymeric architecture on tuning the biological properties of NPs, providing a critical design cue for DMs as well as other types of polymeric micelles.

## ASSOCIATED CONTENT

### Supporting Information

<sup>1</sup>H NMR spectrum of end-group-modified PDCs, TEM images of surface-modified DMs, and confocal images of MCF-7 cells treated with surface-modified DMs, KB cells treated with dual-dye micelles at various time points, and structural integrity of

FRET-micelles in PBS. This material is available free of charge via the Internet at <http://pubs.acs.org>.

## AUTHOR INFORMATION

### Corresponding Author

\*Phone 312-413-8294; Fax 312-996-0098; e-mail [sphong@uic.edu](mailto:sphong@uic.edu) (S.H.).

### Notes

The authors declare no competing financial interest.

## ACKNOWLEDGMENTS

This work was supported by the Hans W. Vahlteich Research Fund from the University of Illinois at Chicago (UIC), NCI/NIH (grant 1R01CA182528), NSF (grant DMR-1409161), Alex's Lemonade Stand Foundation for Childhood Cancer, and Leukemia & Lymphoma Society. The MD simulation work performed by P.K. was supported by the NSF-DMR (grant 1309765). The research was conducted in a facility constructed with support from the NIH (grant C06RR15482). R.M.P. was partially supported by Dean's Scholarship from UIC.

## REFERENCES

- (1) van Vlerken, L. E.; Vyas, T. K.; Amiji, M. M. *Pharm. Res.* **2007**, *24*, 1405–1414.
- (2) Roberts, M. J.; Bentley, M. D.; Harris, J. M. *Adv. Drug Delivery Rev.* **2002**, *54*, 459–476.
- (3) Harris, J. M.; Chess, R. B. *Nat. Rev. Drug Discovery* **2003**, *2*, 214–221.
- (4) Yu, S. S.; Lau, C. M.; Thomas, S. N.; Jerome, W. G.; Maron, D. J.; Dickerson, J. H.; Hubbell, J. A.; Giorgio, T. D. *Int. J. Nanomed.* **2012**, *7*, 799–813.
- (5) Steinmetz, N. F.; Manchester, M. *Biomacromolecules* **2009**, *10*, 784–792.
- (6) Cruz, L. J.; Tacke, P. J.; Fokkink, R.; Figdor, C. G. *Biomaterials* **2011**, *32*, 6791–6803.
- (7) Leroueil, P. R.; Berry, S. A.; Duthie, K.; Han, G.; Rotello, V. M.; McNerny, D. Q.; Baker, J. R., Jr.; Orr, B. G.; Holl, M. M. *Nano Lett.* **2008**, *8*, 420–424.
- (8) Hong, S.; Leroueil, P. R.; Majoros, I. J.; Orr, B. G.; Baker, J. R.; Banaszak Holl, M. M. *Chem. Biol.* **2007**, *14*, 107–115.
- (9) Yang, Y.; Sunoqrot, S.; Stowell, C.; Ji, J.; Lee, C.-W.; Kim, J. W.; Khan, S. A.; Hong, S. *Biomacromolecules* **2012**, *13*, 2154–2162.
- (10) Albertazzi, L.; Serresi, M.; Albanese, A.; Beltram, F. *Mol. Pharmaceutics* **2010**, *7*, 291–298.
- (11) Duncan, R.; Izzo, L. *Adv. Drug Delivery Rev.* **2005**, *57*, 2215–2237.
- (12) Hong, S.; Bielinska, A. U.; Mecke, A.; Keszler, B.; Beals, J. L.; Shi, X.; Balogh, L.; Orr, B. G.; Baker, J. R.; Banaszak Holl, M. M. *Bioconjugate Chem.* **2004**, *15*, 774–782.
- (13) Hong, S.; Hessler, J. A.; Banaszak Holl, M. M.; Leroueil, P.; Mecke, A.; Orr, B. G. *J. Chem. Health Saf.* **2006**, *13*, 16–20.
- (14) Kitchens, K. M.; Kolhatkar, R. B.; Swaan, P. W.; Ghandehari, H. *Mol. Pharmaceutics* **2008**, *5*, 364–369.
- (15) Leroueil, P. R.; Hong, S.; Mecke, A.; Baker, J. R.; Orr, B. G.; Banaszak Holl, M. M. *Acc. Chem. Res.* **2007**, *40*, 335–342.
- (16) Perumal, O. P.; Inapagolla, R.; Kannan, S.; Kannan, R. M. *Biomaterials* **2008**, *29*, 3469–3476.
- (17) Hong, S.; Rattan, R.; Majoros, I. J.; Mullen, D. G.; Peters, J. L.; Shi, X.; Bielinska, A. U.; Blanco, L.; Orr, B. G.; Baker, J. R., Jr.; Holl, M. M. *Bioconjugate Chem.* **2009**, *20*, 1503–1513.
- (18) Bae, J. W.; Pearson, R. M.; Patra, N.; Sunoqrot, S.; Vuković, L.; Král, P.; Hong, S. *Chem. Commun.* **2011**, *47*, 10302–10304.
- (19) Pearson, R. M.; Patra, N.; Hsu, H. J.; Uddin, S.; Kral, P.; Hong, S. *ACS Macro Lett.* **2013**, *2*, 77–81.
- (20) Sunoqrot, S.; Bae, J. W.; Pearson, R. M.; Shyu, K.; Liu, Y.; Kim, D.-H.; Hong, S. *Biomacromolecules* **2012**, *13*, 1223–1230.
- (21) Sunoqrot, S.; Liu, Y.; Kim, D.-H.; Hong, S. *Mol. Pharmaceutics* **2013**, *10*, 2157–2166.
- (22) Lu, J.; Owen, S. C.; Shoichet, M. S. *Macromolecules* **2011**, *44*, 6002–6008.
- (23) Phillips, J. C.; Braun, R.; Wang, W.; Gumbart, J.; Tajkhorshid, E.; Villa, E.; Chipot, C.; Skeel, R. D.; Kale, L.; Schulten, K. *J. Comput. Chem.* **2005**, *26*, 1781–1802.
- (24) Vanommeslaeghe, K.; Hatcher, E.; Acharya, C.; Kundu, S.; Zhong, S.; Shim, J.; Darian, E.; Guvench, O.; Lopes, P.; Vorobyov, I.; Mackerell, A. D., Jr. *J. Comput. Chem.* **2010**, *31*, 671–690.
- (25) Vorobyov, I.; Anisimov, V. M.; Greene, S.; Venable, R. M.; Moser, A.; Pastor, R. W.; MacKerell, A. D. *J. Chem. Theory Comput.* **2007**, *3*, 1120–1133.
- (26) Darden, T.; York, D.; Pedersen, L. J. *Chem. Phys.* **1993**, *98*, 10089–10092.
- (27) Jo, S.; Kim, T.; Iyer, V. G.; Im, W. *J. Comput. Chem.* **2008**, *29*, 1859–1865.
- (28) Jo, S.; Lim, J. B.; Klauda, J. B.; Im, W. *Biophys. J.* **2009**, *97*, 50–58.
- (29) Nagarajan, R. *Langmuir* **2002**, *18*, 31–38.
- (30) Rosen, M. J. *Surfactants and Interfacial Phenomena*, 3rd ed.; Wiley: Hoboken, NJ, 2004; p 113.
- (31) Vukovic, L.; Khatib, F. A.; Drake, S. P.; Madriaga, A.; Brandenburg, K. S.; Kral, P.; Onyuksel, H. *J. Am. Chem. Soc.* **2011**, *133*, 13481–13488.
- (32) Lin, J.; Zhang, H.; Chen, Z.; Zheng, Y. *ACS Nano* **2010**, *4*, 5421–5429.
- (33) Goldberg, D. S.; Ghandehari, H.; Swaan, P. W. *Pharm. Res.* **2010**, *27*, 1547–1557.
- (34) Kitchens, K. M.; Foraker, A. B.; Kolhatkar, R. B.; Swaan, P. W.; Ghandehari, H. *Pharm. Res.* **2007**, *24*, 2138–2145.
- (35) Seib, F. P.; Jones, A. T.; Duncan, R. *J. Controlled Release* **2007**, *117*, 291–300.
- (36) Bolte, S.; Cordelieres, F. P. *J. Microsc.* **2006**, *224*, 213–232.
- (37) Chen, H.; Kim, S.; Li, L.; Wang, S.; Park, K.; Cheng, J. X. *Proc. Natl. Acad. Sci. U. S. A.* **2008**, *105*, 6596–6601.